ADVANCED MATERIALS
www.advmat.de

Scalable Fabrication of Ambipolar Transistors and Radio-Frequency Circuits Using Aligned Carbon Nanotube Arrays

Zhenxing Wang, Shibo Liang, Zhiyong Zhang, Honggang Liu, Hua Zhong, Lin-Hui Ye, Sheng Wang, Weiwei Zhou, Jie Liu, Yabin Chen, Jin Zhang, and Lian-Mao Peng**

Electronic devices based on carbon nanotubes (CNTs) have attracted significant attention for potential radio frequency (RF) applications.[1–3] It has been shown that intrinsic current-gain and power-gain cutoff frequencies (f_T and f_{max}) above 1 THz should be possible, but experimental demonstration using field-effect transistors (FETs) based on individual CNTs has suffered from excessive parasitic effects and impedance mismatch problems.[2,3] In order to overcome these limitations, great efforts have been concentrated on FETs made from aligned arrays of CNTs.[4,5] Since all of the published A-CNT RF circuits were designed to work in the linear region, it is often stated that it is necessary to use dense arrays of all-semiconducting nanotubes to achieve high performance.[2] While impressive progress has been made in achieving high-density arrays of CNTs,[6–12] for example in several cases the required density of tens of nanotubes per micrometer has been realized, it is still challenging to eliminate all metallic CNTs without damaging semiconducting CNTs and thus severely degrading the performance of the CNT-array FETs.[11–16] Therefore most of the published RF integrated circuits based on CNT array on quartz only can operated at a relative low frequency far below 1 GHz owing to the low cut-off frequency of FETs. Here we argue that rather than trying to avoid the requirement of pure semiconducting CNTs, we may indeed make a good use of natural growing CNTs for RF applications. We demonstrate that perfect ambipolar modulation may be achieved using FETs based on as-grown CNTs arrays on quartz near the minimum current point (MCP). Using the ambipolar region rather than the linear region of these FETs, RF circuits including frequency multipliers and mixers are batch-fabricated and shown to retain their function up to 40 GHz, outperforming all previously reported carbon-based RF circuits.

The core device in our RF circuits is a FET fabricated on a horizontally aligned large-diameter (about 2.4 nm on average) SWCNT arrays. The carrier mobility in the CNT is known to increase rapidly with increasing tube diameter, making the large-diameter CNTs more suitable for RF applications.[17] The geometry of the RF FET is illustrated in **Figure 1**a, where the source (S) electrodes are connected to the common ground and the double parallel gate (G) fingers and drain (D) electrodes are used for the input and output ports, respectively. Figure 1b is an optical image showing arrays of fabricated FETs, and Figures 1c and d are, respectively, low-magnification optical microscope and high-magnification scanning electron microscope (SEM) images showing the detailed electrode structure of the FETs.

The transfer characteristics of the fabricated FET shows ambipolar behavior (Figure 1e) in the sense that the branch at positive gate voltage (n-branch) and that at negative gate (p-branch) are symmetric about the MCP. Owing to the participation of metallic CNTs, as well as the large diameter of the CNTs,[10] the transfer characteristics shown in Figure 1e have a current on/off ratio of less than 1.5, which is comparable to that of graphene top-gated FETs.[18,19] Although low current on/off ratio would preclude applications in digital logic, it is acceptable in analogous RF systems where the device operates in a narrow range of voltage around a fixed point. It should be noted that Ti contacts and a high-efficiency top gate were used here to improve the symmetry between n- and p-branches in transfer characteristics owing to the suitable work function of Ti and high gate efficiency of Y_2O_3 insulator.[20,21] When V_{ds} is fixed at 1 V, as in Figure 1e, the drain current I_{ds} is modulated by gate voltage V_{gs} and varies between 1.31 and 0.94 mA, which corresponds to a channel resistance ranged from 780 to 1060 Ω. The transfer characteristics shown in Figure 1e are very similar to those measured from a graphene FET, and the corresponding output characteristics (Figure 1f) show a saturation tendency at large bias, which is difficult to realize in graphene FETs.[22,23] Sixty-two FETs were batch-fabricated directly on the quartz wafer. Among these FETs only three failed to behave as ambipolar FETs, leading to a yield of over 95%, although there is current variation among the working devices due to the variation in the density of the as-grown CNT arrays (see Figure S1 in the Supporting Information). The yield and uniformity of the CNT devices could be further improved if the uniformity of the CNT density is improved. We found, based on a random test all over the wafer, that a well-behaved ambipolar property

Dr. Z. Wang, S. Liang, Dr. Z. Zhang, H. Zhong, Dr. L.-H. Ye, Dr. S. Wang, Prof. L.-M. Peng
Key Laboratory for the Physics and Chemistry of Nanodevices, and Department of Electronics
Peking University
Beijing, 100871, PR China
E-mail: zyzhang@pku.edu.cn; lmpeng@pku.edu.cn

Dr. H. Liu
Microwave Devices and Integrated Circuits Department
Institute of Microelectronics
Chinese Academy of Sciences
Beijing, 100029, PR China

Dr. W. Zhou, Prof. J. Liu
Department of Chemistry
Duke University
Durham, North Carolina, 27708, USA

Y. Chen, Prof. J. Zhang
Key Laboratory for the Physics and Chemistry of Nanodevices and, College of Chemistry and Molecular Engineering
Peking University
Beijing, 100871, PR China

DOI: 10.1002/adma.201302793

© 2013 WILEY-VCH Verlag GmbH & Co. KGaA, Weinheim

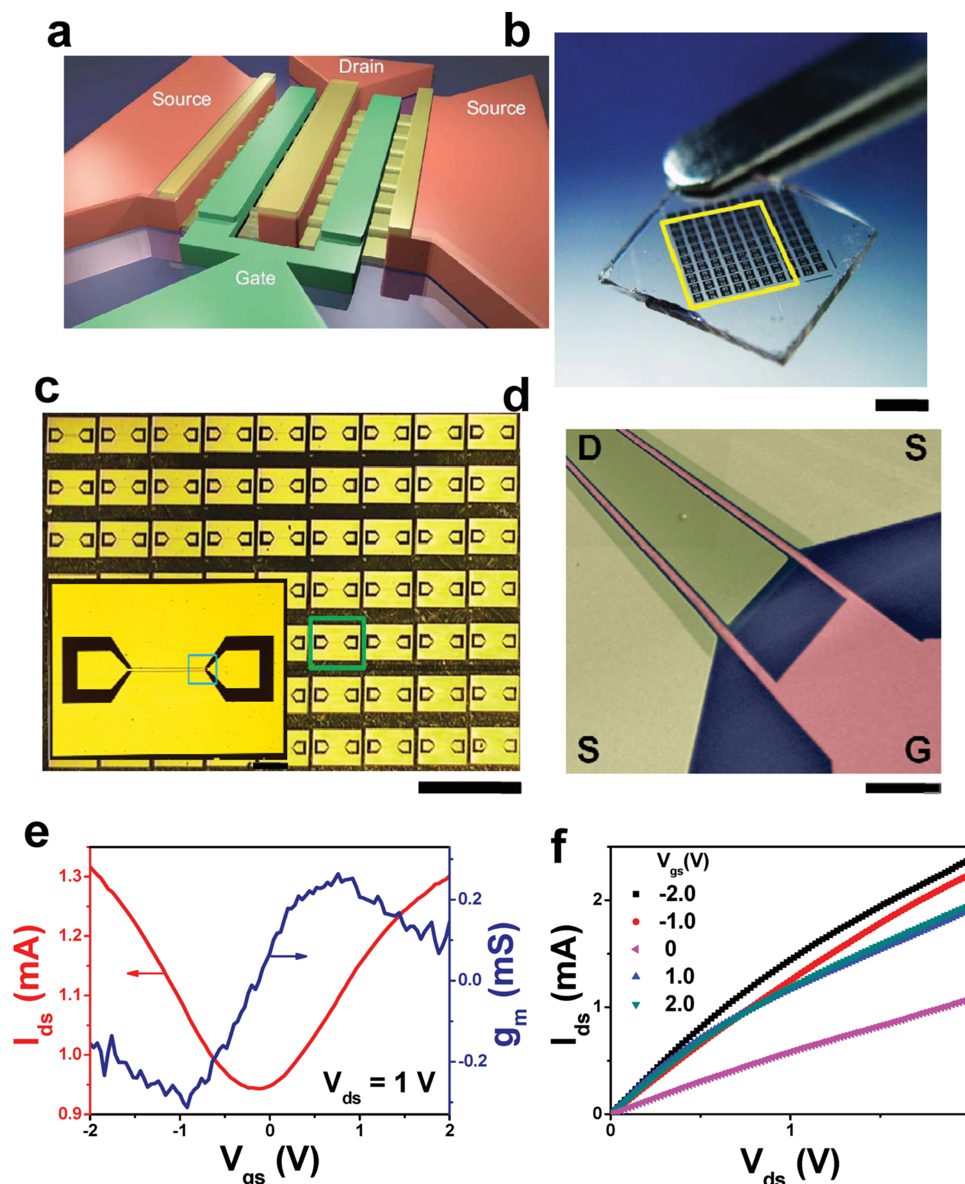

Figure 1. The geometry and DC characteristics of ambipolar CNT FETs. a) Schematic diagram illustrating the geometry of the FET based on CNTs arrays. b) Optical image showing device arrays on a quartz wafer (the scale bar is 2 mm), and, c) enlarged image showing the part of device arrays marked within the yellow box of b. The scale bar is 1 mm. Inset: optical image of a single device marked with green box of c, with a GSG structure for the probing and the core part of the FET. The scale bar is 70 µm. d) SEM image showing the core region of the FET shown in the blue box of the inset of c, with S, D, and G electrodes. The channel length is 1 µm, the gate length is 500 nm, and the gate width is 300 µm. The scale bar is 5 µm. e) DC transfer characteristics of the FET are shown on the left scale, and the corresponding transconductance on the right scale, at bias voltage V_{ds} = 1 V. f) Output characteristics of the FET, with the bias V_{gs} varying from −2 to 2 V with a step of 0.5 V, as indicated in the legend.

ensures normal device function up to high frequencies. During the test we did not observe any FETs that showed good ambipolar transfer characteristic while not being able to function well in RF circuits. The radiofrequency response is also measured, which results in an intrinsic cutoff frequency of 5.3 GHz and maximum oscillation frequency of 2.2 GHz (see Figure S2 in the Supporting Information).

The presence of metallic CNTs in the arrays is generally considered as disadvantageous for RF applications, since it results in large off-state current and thus low on- to off-state current ratio, and reduces the output resistances and thus the gain and frequency of operation. Various strategies have been proposed to selectively remove the metallic CNTs while preserving the semiconducting ones. However all these methods inevitably introduce damage to the remaining semiconducting CNTs and degrade device performance. In this paper, instead of trying to avoid the metallic CNTs, we propose to utilize the mixture of metallic and semiconducting CNTs to introduce small but finite modulation on the conductance. While the modulation is not sufficient for digital electronics, we show that it is well

© 2013 WILEY-VCH Verlag GmbH & Co. KGaA, Weinheim

suited for ambipolar electronics.[21,24,25] Most reported CNT array-based RF devices, such as amplifiers and mixers, explore the on-state incremental linear regime in the transfer characteristic of the FET, with contributions mainly from semiconducting CNTs.[1–5] Although the ambipolar transfer properties had already been observed in some CNT array-based FETs, RF circuits had not not been designed based on the ambipolar properties of CNT arrays. In what follows, we will instead consider the "off-state" ambipolar regime around the MCP where the transfer characteristic of the FET may be described as a harmonic function rather than a linear one (Figure 1e).

Ambipolar RF circuits, including frequency multiplier and mixer, are constructed based on FETs fabricated on wafer-scale horizontally aligned CNT arrays directly grown on quartz. We first consider the frequency multiplier (**Figure 2**a) which is based on an ambipolar CNT FET with transfer characteristics similar to those shown in Figure 1e. When a small RF input signa, l such as $A_0\sin(\omega_0 t)$ with frequency up to 20 GHz, is introduced to the gate of the FET, which is biased at ambipolar region with V_{dc} = –0.2 V, the frequency spectrum of output signal is measured (shown in Figure 2b). Doubling frequency to 40 GHz is obviously presented in the output power spectrum, with more than 10 dBm above the noise background as long as the circuit is powered with a DC voltage V_{dd} = 1 V. The doubling frequency disappeared in the background noise if the power is removed (see Figure S3a in the Supporting Information), demonstrating that the CNT FET can function as an active frequency multiplier with frequency response up to tens of GHz. It should be noted that the 40 GHz response achieved here is not the upper frequency limit of the CNT RF circuit; rather, the upper frequency is limited solely by the measurement apparatus we used.

To analyze the higher order response of the circuit, which is beyond the measurement limit of our apparatus for 20 GHz input signal, the input frequency was lowered to 10 GHz (the corresponding output spectra are shown in Figure S4 in the Supporting Information). The output power $P_{out,2f}$ at doubled frequency 20 GHz increases with input power P_{in} at 10 GHz with a rate of 15 dB per 10 dB (Figure 2c). When plotted in logarithmic scale, the slope between $P_{out,2f}$ and P_{in} is 1.5, which deviates from the ideal slope of 2 (+20 dB per 10 dB) for a perfect frequency doubler. This deviation is due to the fact that the transfer characteristic of the CNT FET (e.g., Figure 1e) is not perfectly harmonic, which tends to saturate at large gate bias,

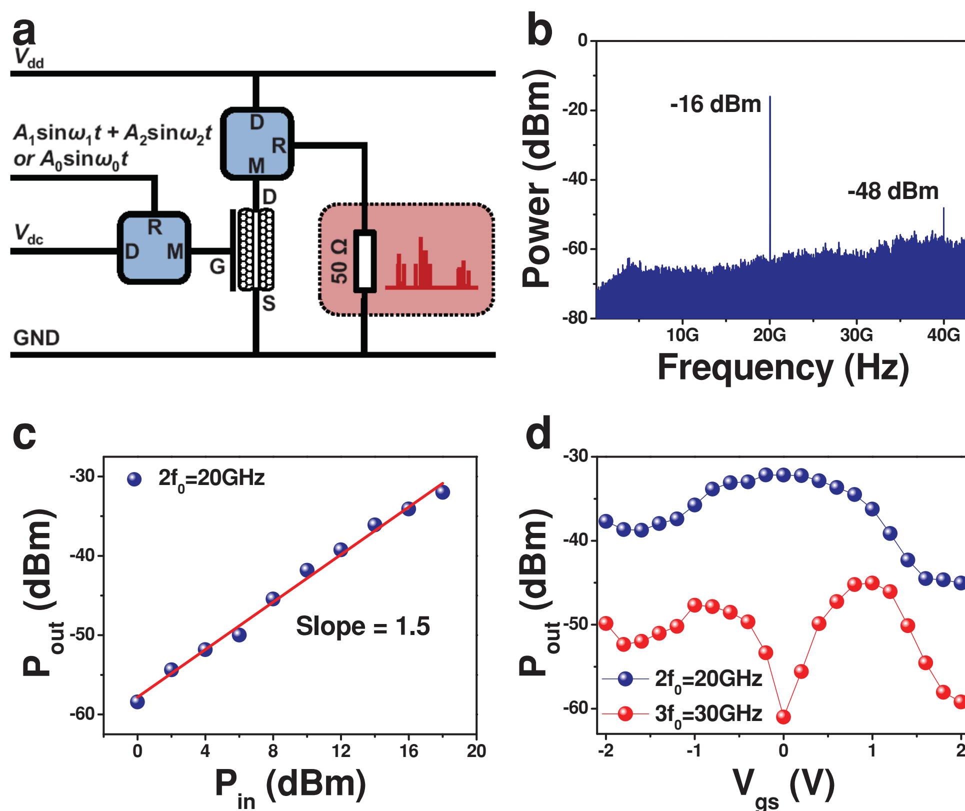

Figure 2. Performance of a CNT frequency multiplier circuit. a) Circuit diagram illustrating the realization of the doubling and mixing functions of the circuit. The gate (G) terminal of the FET is applied with an AC signal as input, either a single-tune signal (for doubling), or a two-tune signal (for mixing), biased with V_{dc} via a bias network (DRM). The drain (D) terminal is biased with V_{dd} and simultaneously connected to a spectrum analyzer for output detection. The source (S) terminal is grounded (GND). b) Output power spectrum for an input signal with a frequency of 20 GHz and a power of 18 dBm. The bias voltage V_{ds} = 1 V, and the gate voltage V_{gs} = –0.2 V. c) Input power dependent output power at doubled frequency (20 GHz). The input signal is with frequency of 10 GHz. The bias voltage V_{ds} = 1 V, and the gate voltage V_{gs} = –0.2 V. d) Input signal gate voltage dependent output power at doubled (20 GHz) and tripled (30 GHz) frequencies. The input signal is with a frequency of 10 GHz and a power of 18 dBm. The bias voltage V_{ds} = 1 V, and the gate voltage V_{gs} varies from –2 V to 2 V.

© 2013 WILEY-VCH Verlag GmbH & Co. KGaA, Weinheim

nevertheless the transfer characteristic is almost symmetric about the MCP. In general, an ideal symmetric transfer curve can be modeled with only even order terms

$$I_{ds} = i_0 + i_2 \left(V_{gs} - V_{MCP}\right)^2 + i_4 \left(V_{gs} - V_{MCP}\right)^4 + \ldots \quad (1)$$

where V_{MCP} is the voltage at the MCP. In reality, certain odd order signals may be generated due to the deviation of the experimental characteristic from the ideal symmetric transfer relation. Figure 2d compares the output powers of doubled frequency (20 GHz) and tripled frequency (30 GHz) for different gate voltages. The output power at tripled frequency (30 GHz) is strongly suppressed by about 29 dBm below the doubled frequency power around $V_{gs} = 0$, where the transfer characteristic reaches the MCP and is almost symmetric about the MCP.

While our CNT circuits are responsive to input signal with frequency up to 20 GHz and generate doubled frequency at output at 40 GHz, as a frequency doubler, the conversion loss (CL) is very high. Figure 2b shows that for an input power of 18 dBm at 20 GHz, the output power at 40 GHz is about –48 dBm, suggesting a CL for doubled frequency of up to 66 dBm. Moreover, the fundamental frequency peak at 20 GHz is also very strong in the output power spectrum, approximately 32 dBm larger than that at the doubled frequency. The large CL may be traced to the small transconductance of less than 1 mS mm^{-1} (e.g., Figure 1e) and the large output resistance of about 800 Ω. The small transconductance is mainly due to the low density of CNTs in the arrays (about 1 CNT μm^{-1}) used for constructing the FET, which may be effectively improved by increasing the CNT density in the arrays and decreasing the channel length.

Another important reason leading to large CL may be the large output resistance of the CNT transistors, which will result in a mismatch between the device and the frequency analyzer (with a characteristic impedance of 50 Ω) and introduce a reflection before the signal entering the instrument. It is worth noting that the output resistance can also be reduced effectively by increasing the density of CNTs in the arrays used for building FETs. **Figure 3**a shows the transfer characteristic of a FET built

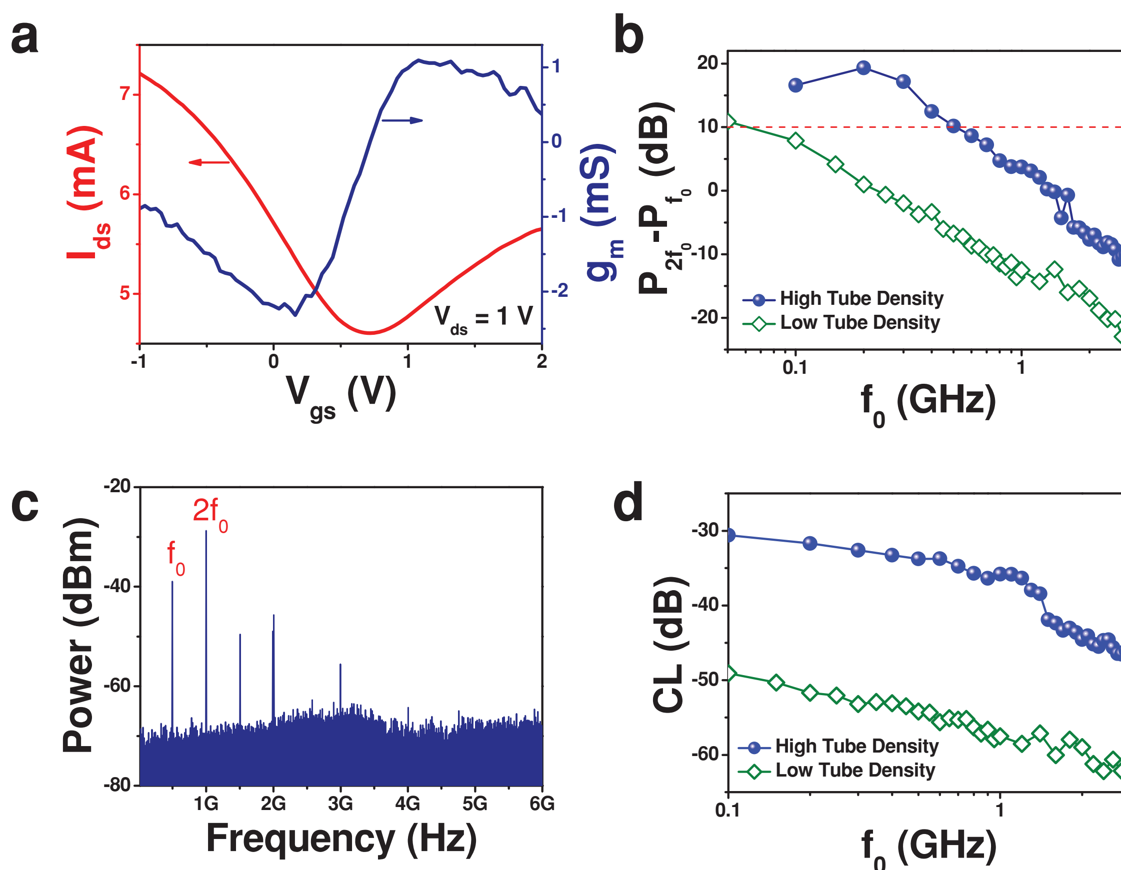

Figure 3. Performance comparisons between CNT RF circuits based on high and low tube density CNTs arrays. a) DC transfer characteristics of a FET with the same geometry as in Figure 1d but is based on CNTs arrays of higher tube density. The drain current is shown with the left side scale, and the corresponding transconductance is shown with the right side scale, with bias voltage V_{ds} = 1 V. b) Input fundamental frequency f_0 dependent power difference P_{2f0}-P_{f0} for circuits based on low and high tube density CNT arrays respectively. For high tube density CNTs arrays, the input signal is with power of 5 dBm. The bias voltage V_{ds} = 1 V, and the gate voltage V_{gs} = 0.6 V. For low tube density CNTs arrays, the input signal is with power of 16 dBm. The bias voltage V_{ds} = 2 V, and the gate voltage V_{gs} = 0 V. The input power and biased condition are all optimized. c) Typical output spectrum for a circuit based on high tube density CNTs arrays. The input signal, with frequency of 500 MHz and power of 5 dBm, is biased at V_{ds} = 1 V, and V_{gs} = 0.6 V. d) Input fundamental frequency dependent conversion loss for devices based on high and low tube density CNTs arrays respectively. The input power and biased condition are the same as in b).

© 2013 WILEY-VCH Verlag GmbH & Co. KGaA, Weinheim

on a CNT array with a density up to about 10 CNT μm^{-1} and diameter of about 1.2 nm (see Figure S5 in the Supporting Information). The transconductance is improved by more than eight times, up to 8 mS mm^{-1}, and output resistance is reduced significantly down to about 120 Ω. Therefore the high-frequency properties are significantly improved, and subsequently the intrinsic cutoff frequency and maximum oscillation frequency are increased to 15.1 and 4.8 GHz, respectively (see Figure S6 in the Supporting Information). However, the transfer characteristic of the device becomes less symmetric, and this is largely due to the use of the smaller diameter (ca. 1.2 nm) CNTs in the device (compared to that used in Figure 1, i.e., 2.4 nm). In general, large-diameter CNTs are more favorable for ambipolar applications.

To quantitatively analyze the performance of the frequency doubler circuit, we use the power difference between the doubled and fundamental frequency, i.e., P_{2f0}– P_{f0}, to scale the spectral purity of the target frequency. The input frequency f_0 dependent power spectra $P_{2f0} - P_{f0}$ for two kinds of CNT FETs are presented in Figure 3b, showing clearly the improvement in the spectral purity when the CNTs arrays density is increased from low (1 CNT μm^{-1}) to high (10 CNT μm^{-1}). Over a wide frequency band, the $P_{2f0} - P_{f0}$ value for the FET with high nanotube density is about 10 dBm larger than that with low nanotube density. In general, a gain in $P_{2f0} - P_{f0}$ of about 10 dBm is required to assure the spectral purity at the doubled frequency of up to 90%, so that the ambipolar circuit as shown in Figure 2 can be used directly as a high-efficiency frequency doubler without using additional filtering circuits. Since $P_{2f0} - P_{f0}$ decreases with increasing f_0, the value of f_0 at which $P_{2f0} - P_{f0}$ = 10 dBm is referred as the critical frequency f_{0c}. Figure 3b shows that f_{0c} is approximately 50 MHz for circuits based on FETs with low CNT density, and this value is larger than 500 MHz for circuits based on FETs with high CNT density. The output power spectrum for the circuit based on high-density CNTs arrays and an input frequency of 500 MHz is shown in Figure 3c, showing clearly that the power at the doubled frequency (1 GHz) P_{2f0} is 10 dBm larger than that at the fundamental frequency P_{f0}. Powers at third, fourth, and higher order frequencies are also visible, but these powers are much lower (by more than 10 dBm) than P_{f0}, and the CNT FET-based ambipolar frequency doubler circuit can operate at GHz with high output spectral purity. Moreover, the CL can also be greatly reduced through increasing the CNT density, as shown in Figure 3d. For the frequency doubler circuit, the CL can be improved by more than 20 dB over a wide frequency range simply by increasing CNT density from low (1 CNT μm^{-1}) to high (10 CNT μm^{-1}). It is expected that the performance of the ambipolar frequency doubler circuit can be significantly improved if state-of-the-art CNT arrays with a density of more than 60 CNT μm^{-1} is used.[8] It should also be noted that the device discussed in this work is not built with a self-aligned gate structure; rather, the FET has a gate length of over 500 nm. Significant performance improvement is expected when the device structure and fabrication processes are optimized, and the gate length is further scaled down.

Frequency mixers, which are widely used in RF system to shift signals from one frequency range to another, can also be readily built based on ambipolar CNT FEFs. The equivalent circuit diagram of a frequency mixer is similar to that shown in Figure 2a for a frequency multiplier, but rather than one signal, two signals with different frequencies, i.e., an RF signal (f_{RF}) and a local oscillator (LO) signal (f_{LO}), are applied to the input port at the gate and intermodulation frequencies (IFs) are generated at the drain as the output. Illustrated in **Figure 4**a is a typical output frequency spectrum when signals with f_{RF} = 20.4 GHz and f_{LO} = 20 GHz are inputted to the mixer, showing clearly the sum frequency peak at $f_{RF} + f_{LO}$ = 40.4 GHz with a power of –44 dBm, the difference frequency peak at $f_{RF} - f_{LO}$ = 400 MHz with a power of –37 dBm, and other peaks with much (at least 14 dBm) lower power, including the third-order IF signals such as $2f_{RF} - f_{LO}$ = 20.8 GHz, $2f_{LO} - f_{RF}$ = 19.6 GHz, and doubling frequencies $2f_{RF}$ = 40.8 GHz and $2f_{LO}$ = 40 GHz.

Due to the measurement limit of the spectrum analyzer we used (up to 43 GHz), input frequencies f_{RF} and f_{LO} are lowered to study the characteristics of IFs. For a fixed RF signal frequency f_{RF} = 15.4 GHz, the LO signal frequency f_{LO} is varied from 10 to 20 GHz, and the f_{LO} dependent behavior of IFs investigated. Generally the sum and difference IF signals are the output frequencies expected from a mixer, while higher-order IF signals should be suppressed. The output power spectrum shown in Figure 4b shows f_{LO} dependent third-order IF, here $2f_{RF} - f_{LO}$, and we see that the third-order IF signal can be significantly suppressed by tuning LO to around 15 GHz. In general, the closer the frequency of the LO signal to RF signal, the better the third-order IF signal suppression. In the limit when f_{LO} is equal to f_{RF}, the mixer becomes a frequency doubler in which the third-order IF signal is not expected for an ideal ambipolar FET with symmetric transfer characteristics. On the other hand, if the third-order IF signal is desired, a moderate adjustment can be made to the LO frequency to increase significantly this IF signal, for example by setting f_{LO} at 12 GHz.

The gate voltage may also have profound effects on the performance of the mixer, especially when the operation of the mixer is based on ambipolar principle. When a signal with f_{RF} = 15.4 GHz and f_{RO} = 15 GHz is applied to the input port of the circuit, an output power spectrum with rich IFs is obtained (see Figure S8 in the Supporting Information). The powers of these IFs are, however, gate dependent. Shown in Figures 4c and d are output powers for all the second- and third-order IF signals, respectively. For all second-order IF signals, including $f_{RF} + f_{LO}$, $f_{RF} - f_{LO}$, $2f_{RF}$, and $2f_{LO}$, the output powers at these frequencies are enhanced when the FET works around the MCP (ca. V_{gs} = 0 V) due to the symmetric nature of the transfer characteristic of the FET. On the other hand, the output powers at third-order and indeed all odd-order IFs are severely lowered around the MCP, typically by about 10 dBm when compared with the second- or other even-order IF signals (Figure 4d).

Besides the intrinsic insulating property of the quartz substrate, which is beneficial for high frequency applications, it is worth noticing that the use of quartz substrate is also critical for achieving better ambipolar characteristics for CNT devices. To prove this statement, we fabricated FETs based on individual CNTs on quartz as well as on that transferred to Si/SiO_2 substrate, although it is challenging due to the high density of CNTs on quartz. For the CNT FETs on quartz, two typical types of transfer characteristics are observed, as shown in **Figures 5**a and b. The one in Figure 5a shows only little

© 2013 WILEY-VCH Verlag GmbH & Co. KGaA, Weinheim

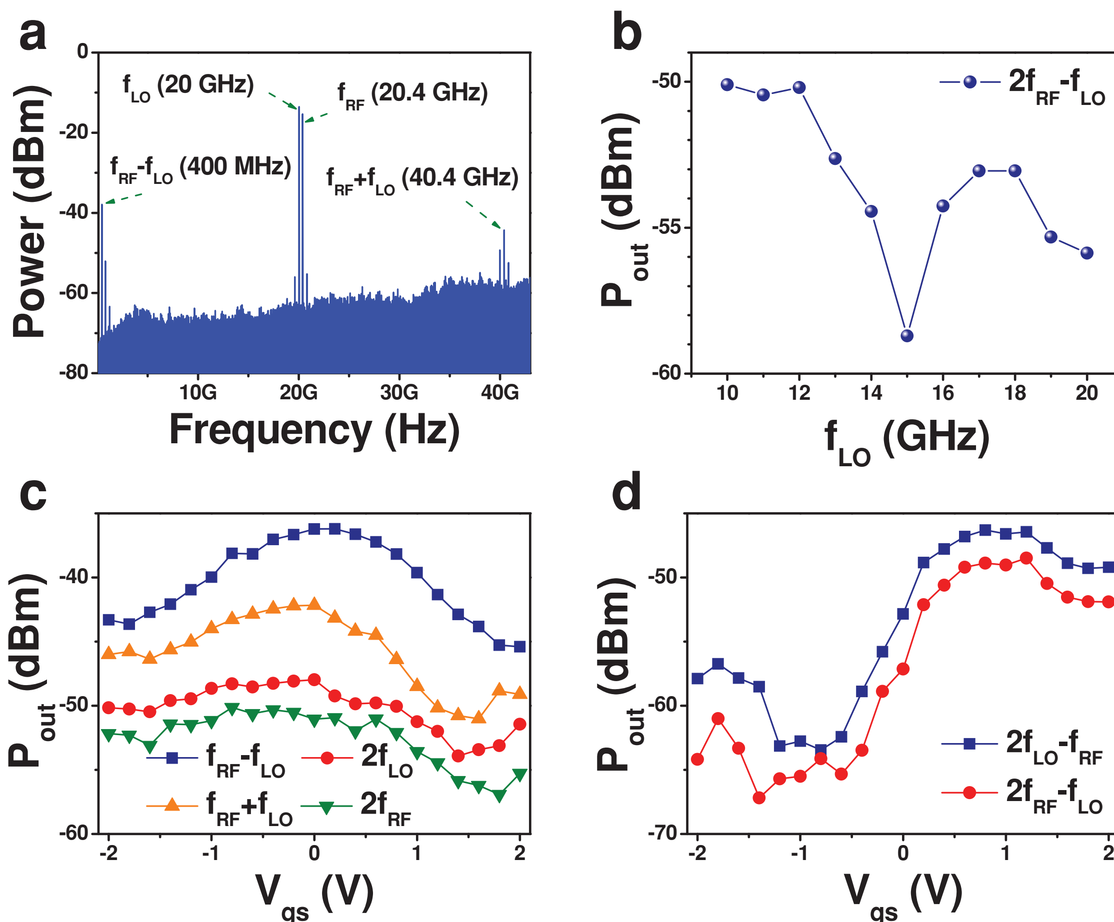

Figure 4. Performance and characteristics of a CNT-based RF mixer. a) Output power spectrum for two input signals: RF signal with frequency of 20.4 GHz, power of 15 dBm, and LO signal with frequency of 20 GHz, power of 18 dBm. The bias voltage V_{ds} = 1 V, and the gate voltage V_{gs} = 0 V. b) LO frequency dependent output power at the third-order IF. The RF signal is with frequency of 15.4 GHz, power of 15 dBm, and the LO signal is with power of 18 dBm. The bias voltage V_{ds} = 1 V, and the gate voltage V_{gs} = 0 V. c) Gate voltage dependent output powers at second-order IFs. The RF signal is with frequency of 15.4 GHz, power of 15 dBm, and the LO signal is with frequency of 15 GHz, power of 18 dBm. The bias voltage V_{ds} = 1 V. d) Gate voltage dependent output powers at third-order IFs. The RF signal is with frequency of 15.4 GHz, power of 15 dBm, and the LO signal is with frequency of 15 GHz, power of 18 dBm. The bias voltage V_{ds} = 1 V.

conductance modulation, and we deduce that the CNT was originally metallic. The other one in Figure 5b shows significant modulation, which can be originated from a semiconducting CNT, and moreover the ambipolar characteristics are obvious even under linear scale for the drain current. It is clear that CNTs show no typical metallic or semiconducting behavior on quartz substrate, while an ambipolar characteristic is usually observed for all CNTs. On the other hand, for the devices fabricated on the CNTs transferred to Si/SiO_2 substrate, typical metallic and semiconducting transfer characteristics are observed, as shown in Figures 5c and d. The behavior of CNT FETs on quartz is obviously different from that on Si/SiO_2 substrate, and we can conclude that the substrate plays an important role here. However, the mechanism behind the observed ambipolar characteristics in real devices based on CNT arrays on quartz is complicated, which needs further studies to reach a solid conclusion on the mechanism.

Although CNTs have all the remarkable properties that an ideal electronic material should have, the potential of CNTs is not fully realized in building nanoelectronic circuits. One of the major obstacles to the further progress of CNT-based nanoelectronics is concerned with the control on the chirality of the CNT, which can be achieved with certain success for short and small diameter CNT but remains challenging for long and large-diameter CNTs.[16,26] By concentrating on the ambipolar rather than unipolar characteristics of the FETs made from aligned arrays of CNTs, here we show that it is possible to realize scalable fabrication of high-performance RF circuits directly on the as-grown thin film of aligned arrays of CNTs. Although it is demonstrated that our ambipolar CNT RF circuits can work up to 40 GHz, with the upper frequency limit determined solely by the measurement system and not the circuit itself, the conversion loss from the input to output is significant. We show that this situation can be greatly improved by increasing the density of CNTs in the arrays, and further significant improvements on the performance of the CNT RF circuits are also anticipated when the device geometry is optimized and channel length is scaled down to submicron level.

© 2013 WILEY-VCH Verlag GmbH & Co. KGaA, Weinheim

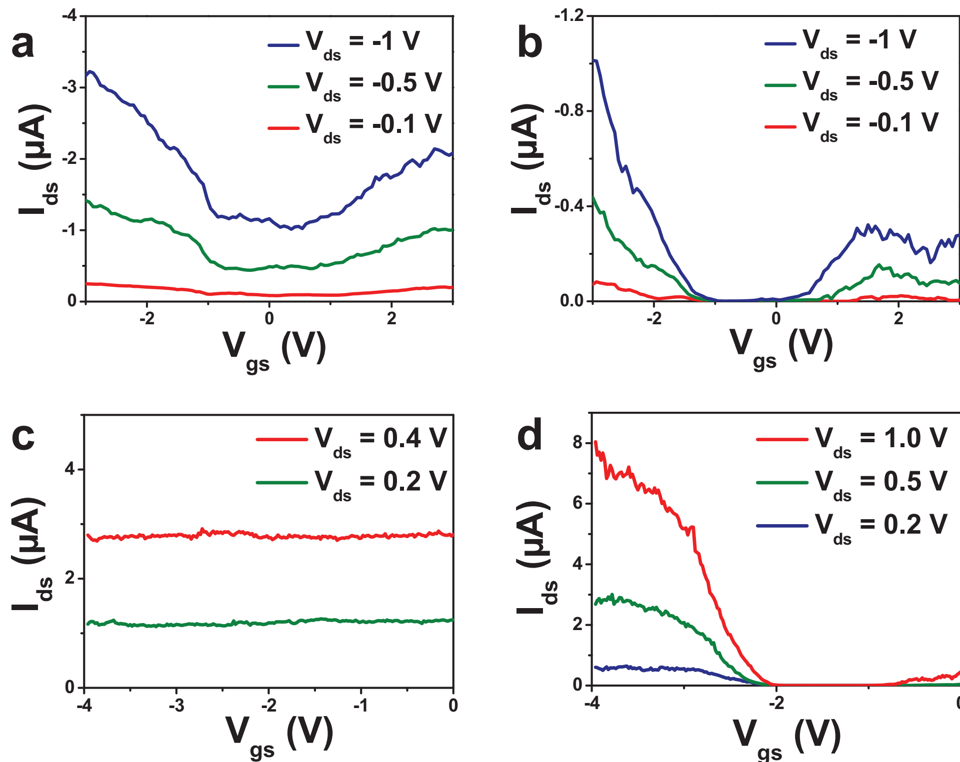

Figure 5. Typical transfer characteristics of FETs based on individual CNTs. The CNTs are grown on quartz, and the transfer characteristics are obtained from: a) a metallic-like FET, and, b) a semiconducting-like FET. The CNTs were grown on quartz and then transferred to Si/SiO_2 substrate, and the transfer characteristics are obtained from: c) a metallic CNT-based FET, and, d) a semiconducting CNT-based FET. The channel length is 1 μm for all devices.

Experimental Section

Perfectly aligned arrays of long single-walled CNTs (SWCNTs) with density of about 1–2 CNTs/μm and diameter distribution of 2.4 ± 0.5 nm (see Figure S9 in the Supporting Information) were grown by multiple-cycle chemical vapor deposition (CVD), which has been shown to preferentially grow high-density and large-diameter carbon nanotubes on stable temperature (ST)-cut quartz substrates.[10] SWCNT arrays with a higher density (greater than 10 per μm) were also grown by CVD, as previously report.[27] The samples of aligned CNTs on Si/SiO_2 substrates were prepared via a standard transferring method.[28] The aligned CNTs were coated with PMMA 600 K, the quartz layers underneath were then dissolved by hydrofluoric acid, and the free-standing PMMA layers were attached to precleaned Si/SiO_2 substrates and removed by acetone. All the structures were realized via e-beam lithography, with the D, S, and G electrodes consisting of Ti/Au 50/50 nm, and a 5 nm thin film of yttrium oxide was utilized as the high-performance gate dielectric.[20] Arrays of devices were directly fabricated using the CNTs arrays on quartz wafer with a size of about 1 cm × 1 cm. During RF measurements, the devices were approached via a ground–signal–ground (GSG) coplanar waveguide using a GSG probing system (see Figure S10 in the Supporting Information).

Supporting Information

Supporting Information is available from the Wiley Online Library or from the author.

Acknowledgements

This work was supported by the Ministry of Science and Technology of China (MOST, grant nos. 2011CB933001 and 2011CB933002), and the National Science Foundation of China (NSFC, grant nos. 61322105, 61271051, and 61376126). The work at Duke is supported by ONR (N00014–09–1–0163) and RF Nano Inc.

Received: June 19, 2013
Revised: August 27, 2013
Published online: October 23, 2013

[1] C. Kocabas, H. Kim, T. Banks, J. A. Rogers, A. A. Pesetski, J. E. Baumgardner, S. V. Krishnaswamy, H. Zhang, *Proc. Natl. Acad. Sci. U. S. A.* **2006**, *105*, 1405.
[2] C. Rutherglen, D. Jain, P. Burke, *Nat. Nanotechnol.* **2009**, *4*, 811.
[3] S. O. Koswatta, A. Valdes-Garcia, M. B. Steiner, Y.-M. Lin, P. Avouris, *IEEE Trans. Microwave Theory Tech.* **2011**, *59*, 2739.
[4] S. J. Kang, C. Kocabas, T. Ozel, M. Shim, N. Pimparkar, M. A. Alam, S. Rotkin, J. A. Rogers, *Nat. Nanotechnol.* **2007**, *2*, 230.
[5] K. Ryu, A. Badmaev, C. Wang, A. Lin, N. Patil, L. Gomez, A. Kumar, S. Mitra, H.-S. P. Wong, C. Zhou, *Nano Lett.* **2009**, *9*, 189.
[6] C. Kocabas, S.-H. Hur, A. Gaur, M. A. Meitl, M. Shim, J. A. Rogers, *Small* **2005**, *1*, 1110.
[7] W. W. Zhou, C. Rutherglen, P. J. Burke, *Nano Res.* **2008**, *1*, 158.
[8] L. Ding, D. N. Yuan, J. Liu, *J. Am. Chem. Soc.* **2008**, *130*, 5428.

© 2013 WILEY-VCH Verlag GmbH & Co. KGaA, Weinheim

[9] N. Patil, A. Lin, E. R. Myers, K. Ryu, A. Badmaev, C. Zhou, H.-S. P. Wong, S. Mitra, *IEEE Trans. Nanotechnol.* **2009**, *8*, 498.
[10] W. Zhou, L. Ding, S. Yang, J. Liu, *ACS Nano* **2011**, *5*, 3849.
[11] C. Wang, K. M. Ryu, L. G. D. Arco, A. Badmaev, J. L. Zhang, X. Lin, Y. C. Che, C. W. Zhou, *Nano Res.* **2010**, *3*, 831.
[12] S. Shekhar, P. Stokes, S. I. Khondaker, *ACS Nano* **2011**, *5*, 1739.
[13] P. G. Collins, M. S. Arnold, P. Avouris, *Science* **2001**, *292*, 706.
[14] G. Zhang, P. Qi, X. Wang, Y. Lu, X. Li, R. Tu, S. Bangsaruntip, D. Mann, L. Zhang, H. Dai, *Science* **2006**, *314*, 974.
[15] L, Ding, A. Tselev, J. Wang, D. Yuan, H. Chu, T. P. McNicholas, Y. Li, J. Liu, *Nano Lett.* **2009**, *9*, 800.
[16] M. C. Hersam, *Nat. Nanotechnol.* **2008**, *3*, 387.
[17] X. J. Zhou, J.-Y. Park, S. M. Huang, J. Liu, P. L. McEuen, *Phys. Rev. Lett.* **2005**, *95*, 146805.
[18] L. Liao, Y.-C. Lin, M. Bao, R. Cheng, Y. Liu, Y. Qu, K. L. Wang, Y. Huang, X. Duan, *Nature* **2010**, *467*, 305.
[19] Y.-M. Lin, A. Valdes-Garcia, S.-J. Han, D. B. Farmer, I. Meric, Y. Sun, Y. Wu, C. Dimitrakopoulos, A. Gill, P. Avouris, K. A. Jenkins, *Science* **2011**, *332*, 1294.
[20] Z. Wang, H. Xu, Z, Zhang, S. Wang, L. Ding, Q. Zeng, L. Yang, T. Pei, M. Gao, L.-M. Peng, *Nano Lett.* **2010**, *10*, 2024.
[21] Z. Wang, L. Ding, T. Pei, Z. Zhang, S. Wang, T. Yu, X. Ye, F. Peng, Y. Li, L.-M. Peng, *Nano Lett.* **2010**, *10*, 3648.
[22] I. Meric, M. Y. Han, A. F. Young, B. Ozyilmaz, P. Kim, K. L. Shepard, *Nat. Nanotechnol.* **2008**, *3*, 654.
[23] S.-J. Han, K. A. Jenkins, A. V. Garcia, A. D. Franklin, A. A. Bol, W. Haensch, *Nano Lett.* **2011**, *11*, 3690.
[24] T. Palacios, *Nat. Nanotechnol.* **2011**, *6*, 464.
[25] L. Liao, J. Bai, R. Cheng, H. Zhou, L. Liu, Y. Liu, Y. Huang, X. Duan, *Nano Lett.* **2012**, *12*, 2653.
[26] X. Tu, S. Manohar, A. Jagota, M. Zheng, *Nature* **2009**, *460*, 250.
[27] Y. Chen, Y. Hu, Y. Fang, P, Li, C. Feng, J. Zhang, *Carbon* **2012**, *50*, 3295.
[28] Q. Zeng, S. Wang, L. Yang, Z. Wang, T. Pei, Z. Zhang, L.-M. Peng, W. Zhou, J. Liu, W. Zhou, *Opt. Mater. Express* **2012**, *2*, 839.

© 2013 WILEY-VCH Verlag GmbH & Co. KGaA, Weinheim